Earth and Planetary Science Letters 416 (2015) 67–72

Contents lists available at ScienceDirect

Earth and Planetary Science Letters

www.elsevier.com/locate/epsl

The coordination and distribution of B in foraminiferal calcite

Oscar Branson [a,b,*], Karina Kaczmarek [c], Simon A.T. Redfern [a], Sambuddha Misra [a], Gerald Langer [a], Tolek Tyliszczak [c], Jelle Bijma [d], Henry Elderfield [a]

[a] Department of Earth Sciences, University of Cambridge, Downing Street, Cambridge CB2 3EQ, UK
[b] Earth and Planetary Sciences, 2119 Earth and Physical Sciences, UC Davis, One Shields Avenue, Davis, CA 95616, USA
[c] Advance Light Source, BL 11.0.2, One Cyclotron Road, MS 6R2100, Berkeley, CA 94720, USA
[d] Alfred Wegener Institute, Helmholtz Centre for Polar and Marine Research, Am Handelshafen 12, D-27570 Bremerhaven, Germany

ARTICLE INFO

Article history:
Received 2 September 2014
Received in revised form 6 February 2015
Accepted 8 February 2015
Available online 25 February 2015
Editor: G.M. Henderson

Keywords:
$\delta^{11}B$
B/Ca
boron
foraminifera
biomineralisation
palaeoproxy

ABSTRACT

The isotopic ratio and concentration of B in foraminiferal calcite appear to reflect the pH and bicarbonate concentration of seawater. The use of B as a chemical proxy tracer has the potential to transform our understanding of the global carbon cycle, and ocean acidification processes. However, discrepancies between the theory underpinning the B proxies, and mineralogical observations of B coordination in biomineral carbonates call the basis of these proxies into question. Here, we use synchrotron X-ray spectromicroscopy to show that B is hosted solely as trigonal BO_3 in the calcite test of *Amphistegina lessonii*, and that B concentration exhibits banding at the micron length scale. In contrast to previous results, our observation of trigonal B agrees with the predictions of the theoretical mechanism behind B palaeoproxies. These data strengthen the use of B for producing palaeo-pH records. The observation of systematic B heterogeneity, however, highlights the complexity of foraminiferal biomineralisation, implying that B incorporation is modulated by biological or crystal growth processes.

1. Introduction

The mineral tests of foraminifera, a ubiquitous group of marine protozoa, record the physical and chemical state of the oceans in which they grow (Lea, 2003). These carbonate archives of ocean chemistry may be preserved in marine sediments for millions of years, providing detailed environmental records key to our understanding of past, present and future climate changes (Elderfield et al., 2006; Lea, 2003). The isotopic ratio and concentration of B in foraminiferal calcite appear to reflect the pH and bicarbonate concentration of seawater, respectively (Allen et al., 2012; Hemming and Hanson, 1992; Yu et al., 2007), and are important for our understanding of the ocean carbon system, and ocean acidification processes (Raven et al., 2005). However, discrepancies between the theory underpinning the B proxies (Hemming and Hanson, 1992) and experimental observations of B coordination (Klochko et al., 2009; Rollion-Bard et al., 2011; Sen et al., 1994) in carbonates undermine our confidence in these important proxies.

Boron in seawater exists in a pH-dependent equilibrium between two aqueous species: the neutral, trigonal planar $B(OH)_3$, and the larger anionic, tetrahedral $B(OH)_4^-$ (Hershey et al., 1986). The greater bond strength of $B(OH)_3$ leads to a partitioning of heavy ^{11}B in the trigonal species, following the principles of equilibrium isotope fractionation (Hemming and Hanson, 1992; Urey, 1947). This drives a pH-dependent shift in the $\delta^{11}B^i$ of each species. Marine carbonate minerals incorporate trace amounts of B, which endows them with the ability to record the state of the seawater B equilibrium, and consequently the pH and carbonate chemistry of seawater (Hemming and Hanson, 1992; Yu et al., 2007). The ability of a carbonate mineral to retain the state of the seawater B equilibrium hinges on the sole uptake of a single B species from seawater. Based on the B isotopic composition of biomineral and inorganic carbonates relative to the seawater they were produced in, the B palaeoproxies assume the sole incorporation of seawater $B(OH)_4^-$ into foraminiferal calcite (Hemming and Hanson, 1992; Ruiz-Agudo et al., 2012). However, pH-sensitive offsets exist in the $\delta^{11}B$ of carbonates that confound this ideal relationship. These offsets could either be driven by some aspect of the biomineralisation process, or by the concomitant uptake of $B(OH)_3$ alongside $B(OH)_4^-$ into the growing calcite. If an unknown proportion of $B(OH)_3$ is incorporated alongside $B(OH)_4^-$, it renders the proxy data uninterpretable, as numerous crystal

* Corresponding author at: Earth and Planetary Sciences, 2119 Earth and Physical Sciences, UC Davis, One Shields Avenue, Davis, CA 95616, USA. Tel.: +1 530 220 2650.
E-mail address: oscarbranson@gmail.com (O. Branson).

http://dx.doi.org/10.1016/j.epsl.2015.02.006

growth and biological parameters would influence the partitioning of B species into the mineral. Many calibration studies support the notion that only borate is incorporated (Allen et al., 2012; Henehan et al., 2013; Rae et al., 2011; Sanyal et al., 2001), but recent nuclear magnetic resonance (NMR) studies suggest that a mixture of both B species is hosted in carbonate biominerals (Klochko et al., 2009; Rollion-Bard et al., 2011). This is at odds with the assumption of incorporation of a single aqueous B species, and raises questions over the suitability of B as a palaeoproxy element. Here, we apply nano-scale X-ray spectromicroscopy techniques to address the fundamental uncertainties surrounding the incorporation of B into biomineral calcite, by conducting a nano-scale mineralogical investigation of the distribution and chemical coordination of B, at a length-scale relevant to biomineralisation processes.

2. Methodology

We characterise the coordination of B in the benthic symbiont-bearing foraminifera *Amphistegina lessonii* using Near-Edge X-ray Absorption Fine Structure (NEXAFS). Specimens were cultured in an elevated (10× ambient) B medium (at the Alfred-Wegener-Institute Helmholtz-Centre for Polar and Marine Research) to raise B concentration above the detection limit of the instrument. Test cross-sections were prepared using a focused ion beam (FIB), and analysed using a scanning transmission x-ray microscope (STXM) at beamline 11.0.2 of the ALS synchrotron (Berkeley, CA).

2.1. Foraminifera culturing

Amphistegina lessonii specimens were obtained from a study by Kaczmarek et al. (2014). Juvenile specimens were transferred into modified filtered North Sea Water (NSW) containing 4.17 mM B (approximately 10× ambient), with the pH titrated back to 8.1 (ambient). Specimens were incubated at 25 °C in a 12/12 light/dark light cycle (light: 100–150 µmol photons m^2 s^{-1}) for three months. Every three days the foraminifera were fed with concentrated, sterilised *Dunaliella salina* algae, and the NSW was replaced. After three months, specimens were bleached in diluted NaOCl:H_2O (1:3) for 6 h, rinsed four times in deionised water, and dried at 50 °C for 12 h. Three *A. lessonii* cultured in two carbonate ion concentrations were analysed in this study, with B/Ca of 5.23 ± 1.06 and 2.95 ± 0.53 mmol/mol B/Ca (treatments $pH8.1^{160}$ and $pH8.1^{260}$ of Kaczmarek et al., 2014). The specimens produced qualitatively identical results (Fig. S1), although the lower B specimens were closer to the detection limit of the instrument, and produced lower quality data than those presented here.

2.2. Sample preparation

Thin-sections for STXM analysis were prepared using a Helios Nanolab focused ion beam (FIB) instrument, following a modified method after Branson et al. (2013). The milling process differed in that the beam energy was reduced throughout the milling process, to minimise sample surface damage. This was necessary because the lower energy of the B K-edge (cf. the Mg K-edge, studied in Branson et al., 2013) necessitated a thinner section, where surface damage became an important consideration. Our FIB sample preparation method was measured by TEM to produce 7.5 nm of amorphous damaged material on each side of the sample (Fig. S2); more than predicted by studies of crystalline silica (Gao et al., 2004; McCaffrey et al., 2001). All STXM analyses were performed on sections between 100–700 nm thick, so this damaged layer comprised 2.1–15% of the analysed material. This will reduce the B signal from foraminiferal calcite, but 85–97.9% of the signal will still be produced by pristine foraminiferal calcite. Previous studies have obtained meaningful STXM and TEM data from FIB-prepared biogenic calcite samples (Benzerara et al., 2011; Branson et al., 2013; Kudo et al., 2010; Obst et al., 2009), and unfocused ion milling instruments have been used previously to thin calcite samples for B analysis (Rollion-Bard et al., 2011), suggesting that this damaged layer will have insignificant impact on our results.

2.3. STXM data acquisition

Data acquisition followed a similar method to Branson et al. (2013). The STXM branch of beamline 11.0.2 at the ALS (Bluhm et al., 2006) has an energy resolution of 0.1 eV, and a spatial resolution of approximately 45 nm (40 nm zone plate) at the B and Mg K-edges. This allowed the extraction NEXAFS spectra from specific, sub-micron regions in the test to examine atomic coordination. The NEXAFS spectrum measures the absorption of X-rays at and above (to +150 eV) the ionisation energy (or 'absorption edge') of an element. The energy of an absorption edge is determined by the electronic structure of the element, allowing us to target specific elements of interest within a material. We examined the 'K-edge' for B and Mg, at approximately 194 eV and 1314 eV, respectively, which results from the excitation of s-shell electrons.

Samples were mounted on aluminium STXM sample holders, which suspended the samples in free space in the X-ray beam. Powder reference materials were applied to X-ray transparent Silson™ 100 nm Si_3N_4 TEM windows for analysis. The sample chamber was evacuated to 40 Pa and flooded with He to 34–50 kPa to minimise X-ray absorption in air. Transmitted X-rays were collected using a scintillation counter, operating in pulse counting mode (Bluhm et al., 2006).

STXM images were taken after a rough NEXAFS spectrum was recorded to precisely locate the absorption edge of B or Mg in the sample. Samples were analysed following a standard procedure: a low-magnification image was taken at the B K-edge to identify interesting patterns in the sample, and smaller regions of interest were imaged at higher magnification, and across the target NEXAFS energy range. All images contained an off-sample region for background (I_0) normalisation and conversion to optical density (OD). The maximum optical density in any spectra was 2.03, below the level where saturation effects are seen on this beamline (above 2.4–2.6). NEXAFS spectra were extracted from image stacks by averaging over the pixels in a region of interest. For the reference materials, if the quality of a single spectrum was poor extra spectra were collected, and data summed to improve quality, effectively increasing the pixel count time.

2.4. STXM data processing and analysis

The position of the absorption edge is influenced by the electronic structure of B, defined by the nearest-neighbour atomic environment (i.e. what elements the B is bonded to, and how they are arranged), and the post-edge features are determined by multiple scattering interactions with the next-nearest-neighbours (the atoms bonded to the nearest-neighbours). The features of a NEXAFS B-spectrum are determined by the coordination of the atom: the number, arrangement, species and coordination of its nearest-neighbour atoms – everything that influences the local electronic environment around the atom of interest. The NEXAFS spectra are particularly sensitive to distinguishing between the coordination states of elements – i.e. between $B(OH)_3$ and $B(OH)_4^-$, which is the focus of our study. In generating Mg maps, we also analysed the Mg K-edge at approximately 1314 eV. The positions of the trigonal and tetrahedral B peaks reported in the literature (Fleet and Liu, 2001; Fleet and Muthupari, 2000, 1999) were confirmed through the analysis of danburite (BO_4) and boric acid (BO_3; Fig. S3). Peak windows identified from these materials were used in generating

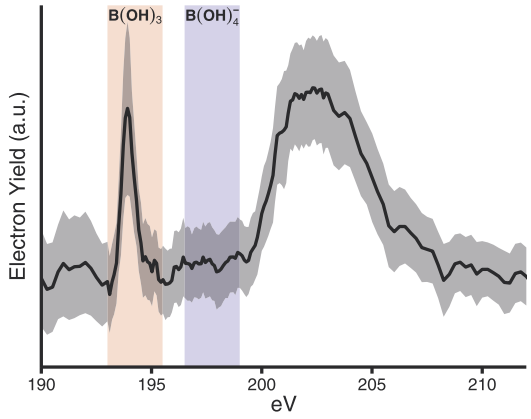

Fig. 1. The mean foraminiferal B spectrum. Only trigonal B was detected in foraminiferal calcite, as indicated by the presence of a strong peak in the trigonal, and no peak in the tetrahedral absorption energy range. The detection threshold for tetrahedral B can be calculated from signal/noise ratios to be 14.9%, thus it is possible to determine that at least 85.1% of B in foraminiferal calcite is in trigonal form.

the B peak maps in Fig. 1. Maps were created following the methods of Branson et al. (2013).

The main data format used in the study was spectral image stacks. An image stack represents a 3D volume of data with spatial x and y dimensions, and a z energy dimension: each pixel in x and y contains a NEXAFS spectrum. Image stacks were collected with a dwell time of 20 ms pixel^{-1} at 162 discrete energies, resulting in a cumulative X-ray exposure time of 3.24 s per stack. Combined with the size of the imaged region, this led to collection times of 6–8 h per stack. Before analysis, image stacks were corrected for sample drift using the 'StackReg' plugin in the Fiji image analysis package (Schindelin et al., 2012; Thevenaz et al., 1998). Aligned image stacks were then imported into the R environment (R Core Team, 2012; RStudio, 2013) for all remaining processing and analysis. During import, image stacks were normalised to I_0, and converted to OD ($-\log(\text{absorption}/I_0)$) before all analysis.

At low energies NEXAFS spectra are complicated by high-order absorption edges of other elements, and their multiple scattering effects. Combined with the heterogeneity of foraminifera test chemistry, each pixel in an image stack has a subtly different background signal beyond the measured I_0, caused by unknown variations in chemistry. To overcome this, the spectrum from each xy pixel in an image stack was independently corrected following the methods of Fleet and Muthupari (2000), who were able to adequately remove significant variations in spectra background from low-B samples. Their correction involved two steps: 1) subtract a linear background based on the pre-edge region, which is assumed to be zero in NEXAFS studies, and 2) subtract a second linear background from the region above peak 'A', based on the data points at the base of peak 'A' (just above 194.5 eV) to the post-spectrum region 20 eV above this (Fig. S4). This method removed the majority of the background signal, leaving easily-comparable, distinct B NEXAFS peaks. Following this correction, peak-intensity maps and spectra were extracted from regions of interest in the sample.

Previous studies of B NEXAFS have revealed the transformation of tetrahedral B to trigonal B to a depth of 6 nm from the surface of B-containing samples (Kasrai et al., 1998; Fleet and Muthupari, 2000; Fleet and Liu, 2001). Should such effects pervade our samples to greater depths they would bias our measurements against the detection of tetrahedral B. However, these surface-specific effects are unlikely be an important factor in our samples for three reasons. First, the surface modification has only been observed in the top 6 nm of B-bearing minerals (Kasrai et al., 1998; Fleet and Liu, 2001), which corresponds to the amorphous FIB-damaged region on our sample surface. Second, our measurements were performed in transmission mode on 'bulk' samples between 100–700 nm thick: equal to or exceeding the penetration depth of 'bulk' measurements of the previous studies (110 nm; Kasrai et al., 1998; Fleet and Liu, 2001), where B coordination transformation was not observed. Finally, measurements of tetrahedral B bearing-danburite (Fig. S3), known to be prone to surface alteration from previous studies (Kasrai et al., 1998; Fleet and Liu, 2001), revealed no trigonal B, despite data being taken from a grain fringe thinner than our foraminiferal samples. Combined with the low X-ray exposure times (no more than a total of 30 s X-ray exposure at each point in the sample during our data collections) compared to previous studies, these factors combine to demonstrate that beam-induced B coordination transformations are not a significant feature in our experiments.

3. Results

The diagnostic trigonal B peak (~194 eV) was present in each xy pixel of the sample. The tetrahedral B peak (~198 eV) was not observed anywhere in the sample. A mean sample spectrum highlights the sole presence of trigonal B in the foraminiferal calcite (Fig. 1). Based on the signal/noise ratio (S/N) of the trigonal B peak, it is possible to estimate the theoretical detection limit of tetrahedral B, assuming similar peak widths and using a standard peak detection threshold of 3N (99.7% confidence), following $3/(3+(\text{S/N}_{\text{trigonal}}))$, where S is the maximum mean peak intensity of the trigonal peak after normalisation, and N is the standard deviation of the background adjacent to the trigonal peak (i.e. the noise). The S/N for the trigonal peak (Fig. 1) is 17.11, giving a tetrahedral B detection threshold of 14.9%. Thus it is possible to determine with 99.7% confidence that 85.1% of B in foraminiferal calcite is in trigonal form. However, this figure represents a conservative estimate of the amount of trigonal B, and with a less stringent peak detection threshold our estimate of % trigonal B increases (89.5% trigonal with 95% confidence, and 94.5% trigonal with 68% confidence). The lack of any suggestion of a peak within energy range over which tetrahedral B appears (Fig. 1), however, implies a complete absence of tetrahedral B in foraminiferal calcite.

The intensity of the peak corresponding to trigonal B varied within the sample, revealing a banded intensity pattern typical of trace element heterogeneity in symbiont-bearing hyaline foraminifera (Fig. 2; Sadekov et al., 2005). However, when compared to an Mg map, a systematic offset between B and Mg bands became evident (Fig. 3).

4. Discussion

Here, we conclusively demonstrate that B is solely hosted in a trigonal coordination in the calcite shell of the benthic foraminifera *Amphistegina lessonii* (Fig. 1). Using Scanning Transmission X-ray Microscopy (STXM) we were able to simultaneously identify the spatial distribution and coordination of B within a microscopic wafer of foraminiferal calcite, at sub-micron spatial resolution. This technique adds a fine spatial aspect to the examination of B coordination, absent from previous studies. Our result is inconsistent with recent NMR data from foraminiferal calcite, which reported ~46% tetrahedral B (Klochko et al., 2009), but is in agreement with the first NMR study performed on carbonate minerals, which reported 80–100% trigonal B in calcite (Sen et al., 1994).

The early NMR study identified tetrahedrally-coordinated B in aragonite, and trigonally coordinated B in calcite (Sen et al., 1994). Sen et al. (1994) observed a coordination change during an aragonite–calcite phase transition, indicating that the atomic

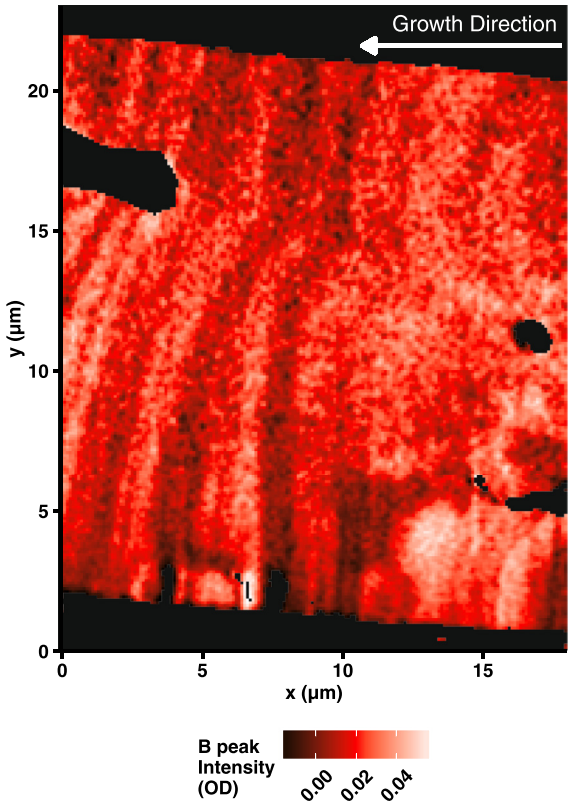

Fig. 2. The distribution of B in foraminiferal calcite, mapped using the intensity of the trigonal B peak (Fig. 1). Peak height is sensitive to B concentration and crystallite orientation, but given that no consistent patterns of crystallite orientation were observed in these specimens, concentration will be the main contributor to this pattern.

structure of the carbonate polymorphs dictates the coordination state of B in the mineral. Our B coordination data adhere to this crystal structure-coordination link, revealing trigonal B in foraminiferal calcite (Fig. 1), although precise details of this structure-coordination link are unknown.

The combination of these early NMR data, and the narrow range of B isotope values across a diverse range of carbonate minerals led to the proposal of a general model of B incorporation in calcite, which underpinned development of the B proxies. This model assumes $B(OH)_4^-$ is attracted to a growth surface where it is either directly incorporated (in aragonite), or de-hydroxylated to a trigonal BO_3^{3-} form during incorporation into calcite (Hemming et al., 1995, 1998). The carbonate mineral thus retains the $\delta^{11}B$ of seawater $B(OH)_4^-$, and a B concentration that reflects the $B(OH)_4^-/HCO_3^-$ ratio of seawater (Hemming and Hanson, 1992; Yu et al., 2007), in a coordination state determined by the structure of the host mineral. This is consistent with the observed lower partitioning of B into calcite than into aragonite (Hemming et al., 1995), associated with the additional energy barrier to de-hydroxylation during incorporation into calcite.

Recent NMR studies of coral aragonite, foraminiferal calcite and inorganic carbonates appear to suggest a much more complex picture of B incorporation (Klochko et al., 2009; Rollion-Bard et al., 2011): highly variable proportions of trigonal and tetrahedral B were apparent between samples, with no clear trends as a function of mineral polymorph, origin or any other factor. This lack of a consistency in coordination environment calls into question the model of B incorporation in carbonates which has emerged from multiple lines of evidence (Hemming and Hanson, 1992; Hemming et al., 1995, 1998; Sen et al., 1994). Without a clear model of B incorporation in carbonates, palaeo-pH records based on the B

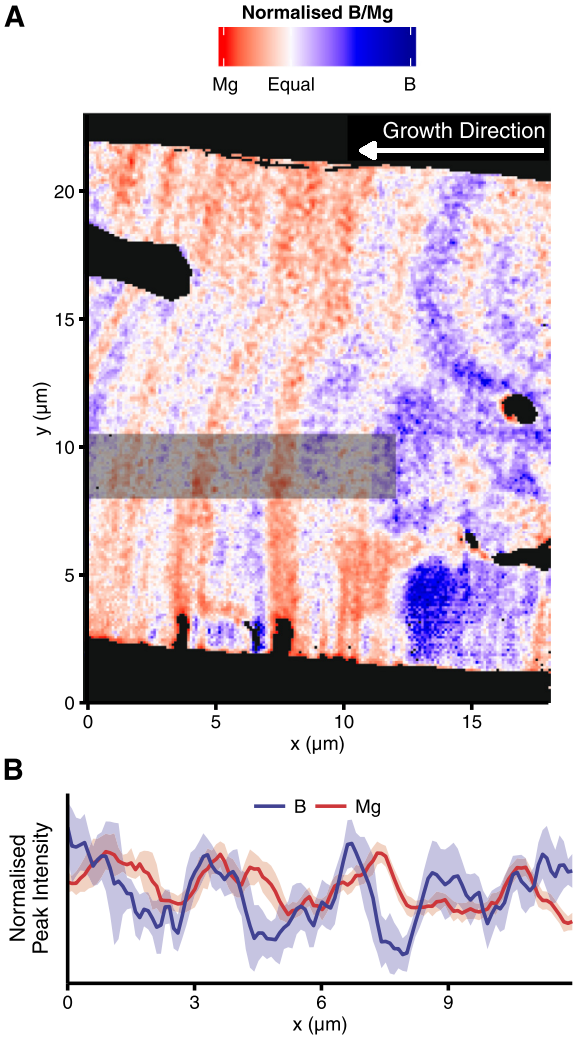

Fig. 3. The relative distribution of Mg and B in foraminiferal calcite. (A) A relative distribution map based on normalised pixel intensity histograms, such that if the distribution of Mg and B were perfectly matched the whole image would be white. (B) The mean normalised B and Mg peak intensities along the direction of growth (x) from the shaded region of interest marked in (A). A cyclic, systematic offset between B and Mg is evident, with peak B concentration occurring after the Mg maximum. This pattern remained similar if the region of interest was shifted in y.

palaeoproxies are reduced to a purely empirical correlation, and become much harder to understand and interpret.

The lack of any systematic coordination trend in recent NMR data either imply that B is indeed incorporated in multiple states in calcite and aragonite (in disagreement with our data, and previously published NMR data; Sen et al., 1994), or that varying amounts of B are hosted in one or more secondary phases in the samples: for example in some interstitial mineral phase, in organic compounds, or in clay particles. NMR techniques average the signal from bulk samples, and in the case of these experiments, required hundreds of mg of powdered material. Given the relatively low concentration of B in carbonates, a single particle of a high-B impurity in the sample would be enough to introduce random offsets in the resulting coordination data, even in the face of the best possible cleaning methods.

Our STXM data allow us to directly address this question, bringing a nano-scale spatial selectivity to our investigation of B coordination. Any secondary phase or contaminant particle could be identified, and excluded (although none were observed in our microscopic sample). Our analyses revealed no tetrahedral B anywhere in the foraminiferal calcite, supporting the earliest NMR

study (Sen et al., 1994). Foraminiferal calcite is known to be compositionally heterogeneous throughout the foraminiferal test. Examination of a region that encapsulates the entire range of compositional heterogeneity can therefore be considered to be representative of the entire structure. Our sample, though very small, contained a representative range of heterogeneity. The observation of persistently homogeneous B coordination across our specimen can therefore be confidently extrapolated to the entire foraminiferal test.

The spatial element of our technique reveals a further trend, which could only be hinted at in past studies (Allen et al., 2011; Hathorne et al., 2009). We observe the systematic banding of B concentration, normal to the direction of shell growth (Fig. 2). Furthermore, this pattern is distinct from the well-documented banding of calcite-bound Mg (Branson et al., 2013) in foraminiferal calcite (Branson et al., 2013; Eggins et al., 2003; Erez, 2003; Hathorne et al., 2009; Sadekov et al., 2005), and appears to be systematically asynchronous (Fig. 3A). We measured both Mg and B X-ray edge spectra for the same area of shell, and found that the Mg concentration maxima are consistently separated from the peaks in B concentration by approximately 1–1.5 μm (Fig. 3B). Previous laser ablation mass spectrometry (LA-ICPMS) studies (Allen et al., 2011; Hathorne et al., 2009) observed various trends in B and Mg concentration at lower spatial resolution, although LA-ICPMS suffers from inherent data 'smoothing', which may have masked the fine scale trends we present here.

Asynchronous banding patterns in foraminiferal calcite could be actively driven by the biological mechanisms that regulate calcification, or caused by passive chemical phenomena that can lead to oscillatory zoning in growing crystals. On the biological side, the pattern could result from changes in $B(OH)_4^-$ concentration driven by fluctuations in calcification site pH (Glas et al., 2012), or by a decoupling of the cation and anion transport mechanisms that regulate Mg and B concentrations (as implied in Nehrke et al., 2013). Both these mechanisms would lead to fluctuations in the bulk fluid chemistry at the calcification site throughout mineralisation. Either of the two main theories describing foraminiferal ion transport (vacuolisation: Bentov et al., 2009; Erez, 2003; and trans-membrane transport: Nehrke et al., 2013) could provide the necessary conditions to vary B concentration or vary pH in the whole calcification environment. Biological mechanisms have recently been shown to influence foraminiferal B/Ca (Babila et al., 2014).

Oscillatory trace element zoning can also arise spontaneously in chemically continuous solutions, through fine-scale interactions in the boundary layer immediately surrounding the calcite growth surface. Banding can arise through self-organisation of impurities to minimise the strain they induce in the crystal structure, by cyclic variations in the boundary layer, driven by the relative diffusion rates of protons and the constituent crystal ions, or by coupled substitution or inhibition interactions between different trace elements (Bryksina et al., 2006; Wang and Merino, 1992). The possible extent of these effects depends on the mineral growth mechanism employed in foraminifera, which remains unknown. The variation in B concentration, whether caused by fluctuations in the calcification environment driven by biological ion transport mechanisms, or by purely chemical oscillatory zoning, serves to demonstrate a poorly-understood complexity underlying foraminiferal calcification. This has implications for all proxies derived from these carbonate climate archives.

The B proxies ($\delta^{11}B$ and B/Ca) have the potential to provide a record of the entire ocean carbonate system throughout Earth history. However, these proxies require the sole incorporation of tetrahedral $B(OH)_4^-$ from seawater, which has thus far been missing in the literature. Our data demonstrate the sole presence of trigonal B in foraminiferal calcite. Intuitively, this does not support the sole incorporation of $B(OH)_4^-$, but our results are predicted by the chemical theory behind the B proxies (Hemming and Hanson, 1992), and the kinetics of B attachment in a growing calcite crystal (Ruiz-Agudo et al., 2012). This theoretical framework describes the re-coordination of tetrahedral $B(OH)_4^-$ to trigonal HBO_3^{2-} during incorporation into the growing mineral. Our coordination data uphold the underlying theory behind the B palaeoproxies, and give a new confidence to the interpretation of B records of past ocean carbonate chemistry. This helps validate their use as a tool to understand ocean carbonate chemistry, and the effects of ocean acidification.

Acknowledgements

We would like to acknowledge David Nicol, Iris Buisman and Martin Walker for invaluable technical assistance, and James Bryson for his help with synchrotron data collection. We would like to thank Jean DeMouthe (California Academy of Sciences) and Mike Rumsey (Natural History Museum, London) for provision of B-containing minerals for use as reference materials. This work was funded by ERC (grant 2010-ADG-267931 to HE), NERC, Jesus College (Cambridge) and the US Department of Energy (via ALS).

Appendix A. Supplementary material

Supplementary material related to this article can be found online at http://dx.doi.org/10.1016/j.epsl.2015.02.006.

References

Allen, K.A., Hönisch, B., Eggins, S.M., Yu, J., Spero, H.J., Elderfield, H., 2011. Controls on boron incorporation in cultured tests of the planktic foraminifer *Orbulina universa*. Earth Planet. Sci. Lett. 309, 291–301.

Allen, K.A., Hönisch, B., Eggins, S.M., Rosenthal, Y., 2012. Environmental controls on B/Ca in calcite tests of the tropical planktic foraminifer species *Globigerinoides ruber* and *Globigerinoides sacculifer*. Earth Planet. Sci. Lett. 351–352, 270–280. http://dx.doi.org/10.1016/j.epsl.2012.07.004.

Babila, T.L., Rosenthal, Y., Conte, M.H., 2014. Evaluation of the biogeochemical controls on B/Ca of *Globigerinoides ruber* white from the Oceanic Flux Program, Bermuda. Earth Planet. Sci. Lett. 404, 67–76. http://dx.doi.org/10.1016/j.epsl.2014.05.053.

Bentov, S., Brownlee, C., Erez, J., 2009. The role of seawater endocytosis in the biomineralization process in calcareous foraminifera. Proc. Natl. Acad. Sci. USA 106, 21500–21504.

Benzerara, K., Menguy, N., Obst, M., Stolarski, J., Mazur, M., Tylisczak, T., Brown Jr., G.E., Meibom, A., 2011. Study of the crystallographic architecture of corals at the nanoscale by scanning transmission X-ray microscopy and transmission electron microscopy. Ultramicroscopy 111, 1268–1275.

Bluhm, H., Andersson, K., Araki, T., Benzerara, K., Brown, G.E., Dynes, J.J., Ghosal, S., Gilles, M.K., Hansen, H.C., Hemminger, J.C., Hitchcock, A.P., Ketteler, G., Kilcoyne, A.L.D., Kneedler, E., Lawrence, J.R., Leppard, G.G., Majzlan, J., Mun, B.S., Myneni, S.C.B., Nilsson, A., Ogasawara, H., Ogletree, D.F., Pecher, K., Salmeron, M., Shuh, D.K., Tonner, B., Tyliszczak, T., Warwick, T., Yoon, T.H., 2006. Soft X-ray microscopy and spectroscopy at the molecular environmental science beamline at the Advanced Light Source. J. Electron Spectrosc. Relat. Phenom. 150, 86–104.

Branson, O., Redfern, S.A.T., Tyliszczak, T., Sadekov, A.Y., Langer, G., Kimoto, K., Elderfield, H., 2013. The coordination of Mg in foraminiferal calcite. Earth Planet. Sci. Lett. 383, 134–141.

Bryksina, N.A., Halden, N.M., Mejia, S., 2006. Qualitative and quantitative characteristics of modeled and natural oscillatory zoning patterns in calcite. Math. Geol. 38, 635–655.

Eggins, S., de Deckker, P., Marshall, J., 2003. Mg/Ca variation in planktonic foraminifera tests: implications for reconstructing palaeo-seawater temperature and habitat migration. Earth Planet. Sci. Lett. 212, 291–306.

Elderfield, H., Yu, J., Anand, P., Kiefer, T., Nyland, B., 2006. Calibrations for benthic foraminiferal Mg/Ca paleothermometry and the carbonate ion hypothesis. Earth Planet. Sci. Lett. 250, 633–649.

Erez, J., 2003. The source of ions for biomineralization in foraminifera and their implications for paleoceanographic proxies. Rev. Mineral. Geochem. 54, 115–149.

Fleet, M.E., Liu, X., 2001. Boron K-edge XANES of boron oxides: tetrahedral B–O distances and near-surface alteration. Phys. Chem. Miner. 28, 421–427.

Fleet, M.E., Muthupari, S., 1999. Coordination of boron in alkali borosilicate glasses using XANES. J. Non-Cryst. Solids 255, 233–241.

Fleet, M.E., Muthupari, S., 2000. Boron K-edge XANES of borate and borosilicate minerals. Am. Mineral. 85, 1009–1021.

Gao, Q., Zhang, M., Niou, C., Li, M., Chien, K., 2004. Sidewall damage induced by FIB milling during TEM sample preparation. In: Annual Proceedings – Reliability Physics (Symposium), pp. 613–614.

Glas, M.S., Langer, G., Keul, N., 2012. Calcification acidifies the microenvironment of a benthic foraminifer (*Ammonia sp.*). J. Exp. Mar. Biol. Ecol. 424–425, 53–58.

Hathorne, E.C., James, R.H., Lampitt, R.S., 2009. Environmental versus biomineralization controls on the intratest variation in the trace element composition of the planktonic foraminifera *G. inflata* and *G. scitula*. Paleoceanography 24, PA4204.

Hemming, N.G., Hanson, G.N., 1992. Boron isotopic composition and concentration in modern marine carbonates. Geochim. Cosmochim. Acta 56, 537–543.

Hemming, N.G., Reeder, R.J., Hanson, G.N., 1995. Mineral–fluid partitioning and isotopic fractionation of boron in synthetic calcium carbonate. Geochim. Cosmochim. Acta 59, 371–379.

Hemming, N.G., Reeder, R.J., Hart, S.R., 1998. Growth-step-selective incorporation of boron on the calcite surface. Geochim. Cosmochim. Acta 62, 2915–2922.

Henehan, M.J., Rae, J.W.B., Foster, G.L., Erez, J., Prentice, K.C., Kucera, M., Bostock, H.C., Martínez-Botí, M.A., Milton, J.A., Wilson, P.A., Marshall, B.J., Elliott, T., 2013. Calibration of the boron isotope proxy in the planktonic foraminifera *Globigerinoides ruber* for use in palaeo-CO_2 reconstruction. Earth Planet. Sci. Lett. 364, 111–122.

Hershey, J.P., Fernandez, M., Milne, P.J., Millero, F.J., 1986. The ionization of boric acid in NaCl, Na–Ca–Cl and Na–Mg–Cl solutions at 25 °C. Geochim. Cosmochim. Acta 50, 143–148.

Kaczmarek, K., Langer, G., Nehrke, G., Horn, I., Misra, S., Janse, M., Bijma, J., 2014. Boron incorporation in the foraminifer *Amphistegina lessonii* under a decoupled carbonate chemistry. Biogeosci. Discuss. 11, 16743–16771.

Kasrai, M., Fleet, M.E., Muthupari, S., Li, D., Bancroft, G.M., 1998. Surface modification study of borate materials from B K-edge X-ray absorption spectroscopy. Phys. Chem. Miner. 25, 268–272.

Klochko, K., Cody, G.D., Tossell, J.A., Dera, P., Kaufman, A.J., 2009. Re-evaluating boron speciation in biogenic calcite and aragonite using ^{11}B MAS NMR. Geochim. Cosmochim. Acta 73 (7), 1890–1900. http://dx.doi.org/10.1016/j.gca.2009.01.002.

Kudo, M., Kameda, J., Saruwatari, K., Ozaki, N., Okano, K., Nagasawa, H., Kogure, T., 2010. Microtexture of larval shell of oyster, *Crassostrea nippona*: a FIB-TEM study. J. Struct. Biol. 169, 1–5.

Lea, D.W., 2003. Elemental and isotopic proxies of past ocean temperatures. In: Elderfield, H., Holland, H.D., Turekian, K.K. (Eds.), The Oceans And Marine Geochemistry. Elsevier, Oxford, p. 365.

McCaffrey, J.P., Phaneuf, M.W., Madsen, L.D., 2001. Surface damage formation during ion-beam thinning of samples for transmission electron microscopy. Ultramicroscopy 87, 97–104.

Nehrke, G., Keul, N., Langer, G., de Nooijer, L.J., Bijma, J., Meibom, A., 2013. A new model for biomineralization and trace-element signatures of foraminifera tests. Biogeosciences 10, 6759–6767.

Obst, M., Dynes, J.J., Lawrence, J.R., Swerhone, G.D.W., Benzerara, K., Karunakaran, C., Kaznatcheev, K., Tyliszczak, T., Hitchcock, A.P., 2009. Precipitation of amorphous $CaCO_3$ (aragonite-like) by cyanobacteria: a STXM study of the influence of EPS on the nucleation process. Geochim. Cosmochim. Acta 73, 4180–4198.

R Core Team, 2012. No title. R Foundation for Statistical Computing. Vienna, Austria.

Rae, J.W.B., Foster, G.L., Schmidt, D.N., Elliott, T., 2011. Boron isotopes and B/Ca in benthic foraminifera: proxies for the deep ocean carbonate system. Earth Planet. Sci. Lett. 302, 403–413. http://dx.doi.org/10.1016/j.epsl.2010.12.034.

Raven, J.A., Caldeira, K., Elderfield, H., Hoegh-Guldberg, O., Liss, P.S., Riebesell, U., Shephard, J.G., Turley, C., Watson, A., 2005. Ocean acidification due to increasing atmospheric carbon dioxide. R. Soc.

Rollion-Bard, C., Blamart, D., Trebosc, J., Tricot, G., Mussi, A., Cuif, J.-P., 2011. Boron isotopes as pH proxy: a new look at boron speciation in deep-sea corals using ^{11}B MAS NMR and EELS. Geochim. Cosmochim. Acta 75, 1003–1012.

RStudio, 2013. RStudio: integrated development environment for R. Version 0.96.330.

Ruiz-Agudo, E., Putnis, C.V., Kowacz, M., Ortega-Huertas, M., Putnis, A., 2012. Boron incorporation into calcite during growth: implications for the use of boron in carbonates as a pH proxy. Earth Planet. Sci. Lett. 345–348, 9–17.

Sadekov, A.Y., Eggins, S.M., de Deckker, P., 2005. Characterization of Mg/Ca distributions in planktonic foraminifera species by electron microprobe mapping. Geochem. Geophys. Geosyst. 6, Q12P06.

Sanyal, A., Bijma, J., Spero, H.J., Lea, D.W., 2001. Empirical relationship between pH and the boron isotopic composition of *Globigerinoides sacculifer*: implications for the boron isotope paleo-pH proxy. Paleoceanography 16, 515–519.

Schindelin, J., Arganda-Carreras, I., Frise, E., Kaynig, V., Longair, M., Pietzsch, T., Preibisch, S., Rueden, C., Saalfeld, S., Schmid, B., Tinevez, J.-Y.Y., White, D.J., Hartenstein, V., Eliceiri, K., Tomancak, P., Cardona, A., 2012. Fiji: an open-source platform for biological-image analysis. Nat. Methods 9, 676–682.

Sen, S., Stebbins, J.F., Hemming, N.G., Ghosh, B., 1994. Coordination environments of B impurities in calcite and aragonite polymorphs: A^{11}B MAS NMR study. Am. Mineral. 79, 819–825.

Thevenaz, P., Ruttimann, U.E., Unser, M., 1998. A pyramid approach to subpixel registration based on intensity. IEEE Trans. Image Process. 7, 27–41.

Urey, H.C., 1947. The thermodynamic properties of isotopic substances. J. Chem. Soc., 562–581.

Wang, Y., Merino, E., 1992. Dynamic model of oscillatory zoning of trace elements in calcite: double layer, inhibition, and self-organization. Geochim. Cosmochim. Acta 56, 587–596.

Yu, J., Elderfield, H., Hönisch, B., 2007. B/Ca in planktonic foraminifera as a proxy for surface seawater pH. Paleoceanography 22, PA2202.